Ultrafast dynamics of adenine following XUV ionization

To cite this article: Erik P Månsson *et al* 2022 *J. Phys. Photonics* **4** 034003

View the article online for updates and enhancements.

Journal of Physics: Photonics

Ultrafast dynamics of adenine following XUV ionization

Erik P Månsson[1,2] , Simone Latini[3], Fabio Covito[3], Vincent Wanie[1,2,4] , Mara Galli[1,5], Enrico Perfetto[6,7], Gianluca Stefanucci[7,8] , Umberto De Giovannini[3,9] , Mattea C Castrovilli[2,10], Andrea Trabattoni[1] , Fabio Frassetto[11] , Luca Poletto[11], Jason B Greenwood[12] , François Légaré[4], Mauro Nisoli[2,5] , Angel Rubio[3,13] and Francesca Calegari[1,2,14,*]

1 Center for Free-Electron Laser Science CFEL, Deutsches Elektronen-Synchrotron DESY, Notkestr. 85, 22607 Hamburg, Germany
2 Institute for Photonics and Nanotechnologies CNR-IFN, P.za L. da Vinci 32, 20133 Milano, Italy
3 Max Planck Institute for the Structure and Dynamics of Matter and Center for Free Electron Laser Science, 22761 Hamburg, Germany
4 INRS-EMT, 1650 Blvd. Lionel Boulet J3X 1S2, Varennes, Canada
5 Department of Physics, Politecnico di Milano, Piazza L. da Vinci 32, 20133 Milano, Italy
6 CNR-ISM, Division of Ultrafast Processes in Materials (FLASHit), Area della ricerca di Roma 1, Via Salaria Km 29.3, I-00016 Monterotondo Scalo, Italy
7 Dipartimento di Fisica, Università di Roma Tor Vergata, Via della Ricerca Scientifica, 00133 Roma, Italy
8 INFN, Sezione di Roma Tor Vergata, Via della Ricerca Scientifica 1, 00133 Roma, Italy
9 Dipartimento di Fisica e Chimica, Università degli Studi di Palermo, Via Archirafi 36, I-90123 Palermo, Italy
10 Istituto di Struttura della Materia-CNR (ISM-CNR), Area della Ricerca di Roma 1, 00015 Monterotondo, Italy
11 Institute for Photonics and Nanotechnologies CNR-IFN, Via Trasea 7, 35131 Padova, Italy
12 Centre for Plasma Physics, School of Maths and Physics, Queen's University Belfast, BT7 1NN Belfast, United Kingdom
13 Center for Computational Quantum Physics (CCQ), The Flatiron Institute, 162 Fifth Avenue, New York, NY 10010, United States of America
14 Institut für Experimentalphysik, Universität Hamburg, Luruper Chaussee 149, D-22761 Hamburg, Germany
* Author to whom any correspondence should be addressed.

E-mail: francesca.calegari@desy.de

Keywords: ultrafast, dynamics, XUV, adenine, nucleobase, dissociation

Abstract

The dynamics of biologically relevant molecules exposed to ionizing radiation contains many facets and spans several orders of magnitude in time and energy. In the extreme ultraviolet (XUV) spectral range, multi-electronic phenomena and bands of correlated states with inner-valence holes must be accounted for in addition to a plethora of vibrational modes and available dissociation channels. The ability to track changes in charge density and bond length during ultrafast reactions is an important endeavor toward more general abilities to simulate and control photochemical processes, possibly inspired by those that have evolved biologically. By using attosecond XUV pulses extending up to 35 eV and few-femtosecond near-infrared pulses, we have previously time-resolved correlated electronic dynamics and charge migration occurring in the biologically relevant molecule adenine after XUV-induced sudden ionization. Here, using additional experimental data, we comprehensively report on both electronic and vibrational dynamics of this nucleobase in an energy range little explored to date with high temporal resolution. The time-dependent yields of parent and fragment ions in the mass spectra are analyzed to extract exponential time constants and oscillation periods. Together with time-dependent density functional theory and *ab-initio* Green's function methods, we identify different vibrational and electronic processes. Beyond providing further insights into the XUV-induced dynamics of an important nucleobase, our work demonstrates that yields of specific dissociation outcomes can be influenced by sufficiently well-timed ultrashort pulses, therefore providing a new route for the control of the multi-electronic and dissociative dynamics of a DNA building block.

1. Introduction

The localization and transport of charge is essential for many photoreactions in biomolecules and functional materials. Just as femtosecond laser technology led to the femtochemistry paradigm, where coherent vibrational wavepackets can be excited and the nuclear motion of molecules be tracked in real time [1, 2], attosecond technology is making it possible to time-resolve electronic dynamics, including multi-electronic transitions with core- or inner-valence holes [3–6] and charge migration across a molecule [7–9]. There is a great interest in utilizing such pulses of light to understand if and how the speed and efficiency of reactions can be improved by better utilizing charge migration and other electronic dynamics, a research field that can be called 'attochemistry' [10–13].

Attosecond pulses are generated via a high-harmonic generation process [14, 15], where a near-infrared (NIR) laser pulse is focused to tunnel-ionize a medium and accelerate electrons away from and then back to their parent ion. The excess kinetic energy of each recombining electron becomes emitted as a photon, which may extend into the extreme ultraviolet (XUV) or soft x-ray regime, depending on the driving laser and medium. Crucially, coherence is preserved from the driving NIR laser to and within the generated attosecond pulse spectrum, allowing pump–probe experiments with sub-femtosecond precision. Attosecond methods based on photoelectron spectroscopy can measure pulse durations [16–18] or time-delays in XUV photoionization processes [19–26] and in the subsequent NIR-probing [27]. Spectroscopy on the initial photoelectron is, however, not sensitive to later dynamics *within* the molecule, for which transient absorption spectroscopy [28, 29] and pump–probe mass spectrometry are often used [30–33].

Charge migration is defined as a net change in electron or hole probability density within a molecule without any accompanying motion of nuclei (which would be called charge transfer instead) [34, 35]. In the mid-1990s it was suggested that this occurred in oligopeptides (short chains of amino acids) after site-selective photoionization [36], based on observations of which charged fragments were obtained. Theoretical work for di- and tetrapeptides showed that a hole could transfer already in 1–5 fs [37, 38]. Such a redistribution of charge within a molecule can in some cases be achieved through a quantum beat of coherently excited orbitals of different energy, while in other cases it must be described as an intrinsic correlation-driven electronic relaxation that lets the occupation of electronic states evolve over time. Experimentally, the use of an isolated attosecond pulse and a few-femtosecond NIR probing pulse has allowed approximately 4 fs periodic charge migration to be confirmed within the single amino acids phenylalanine [7] and tryptophan [39–41].

A related class of biomolecules are DNA-building blocks, such as nucleosides and nucleobases. Attosecond charge migration from one nucleobase to its complementary nucleobase was recently examined in simulations after removing an oxygen-1s electron [42]. Such processes could have direct consequences for the probability of DNA-damage, for which improved control or biological targeting could have applications in radiation therapy of tumors. In general, ionizing radiation is more likely to damage DNA indirectly via radicals and low-energy secondary electrons created when the primary radiation interacts with the much more abundant water molecules in tissue [43–45]. Although the relaxation of DNA-building blocks after 5 eV ultraviolet photoexcitation [46] has been studied extensively with pump–probe cross-correlations of 80–160 fs (features down to 50 fs fitted) [47–51], we are not aware of any time-resolved studies in the 10–50 eV energy range relevant for DNA strand-breakage [43, 52]. The time resolution achieved in the ultraviolet would be insufficient to examine initial inner-valence multi-electronic dynamics as well as any coherently excited vibrational wavepackets and their implications for the structural integrity of the molecule. We have previously reported on the dissociation dynamics of the nucleobase thymine and its nucleoside thymidine ionized by XUV attosecond pulses and probed by few-femtosecond NIR-pulses [53].

In this work, we describe the time-resolved electronic and vibrational dynamics of the nucleobase adenine, ionized by 17–35 eV photons. In the first part, we discuss how XUV-induced charge migration in the adenine cation enables the production of *intact* dications. We use additional experimental data beyond our recent report on this phenomenon [6], which to our knowledge constituted the first photoionization study of adenine above the 23.5 eV dication appearance energy [54]. In the second part, we instead examine the *fragment* ions and discuss signatures of different types of vibrational dynamics. Together, the two parts provide complementary information about the femtosecond dynamics in photoionized adenine.

2. Experimental set-up

Carrier–phase stabilized 25 fs pulses from a titanium:sapphire laser are sent through a hollow-core fiber with a pressure gradient of helium for self-phase modulation, and compressed to 4 fs with a central wavelength of about 700 nm (1.77 eV) by chirped mirrors [55, 56]. A beam splitter gives two replicas of this NIR pulse, one of which is sent through waveplates for polarization gating [57–59] and focused in a pulsed jet of krypton to

generate [14, 15] the XUV isolated attosecond pulse. An aluminum filter is then used to block the residual NIR while transmitting most of the XUV [60]. The resulting attosecond pulse has a duration below 300 as and a continuous XUV spectrum from 17 to 35 eV, with the highest spectral intensity near 27 eV [6]. The other part of the NIR-beam is used as a probe at an estimated intensity of $1-1.4 \times 10^{13}$ W cm^{-2}, recombined collinearly using an annular mirror after a piezoelectric delay-stage to achieve a Mach–Zehnder-like interferometer. To reduce most of the thermal drift, an active stabilization system for the delay is locked onto the spatial fringes of a helium:neon laser that is co-propagating through most of the interferometer (giving an in-loop residual RMS error of 20 as).

Adenine was sublimated at 190 °C with helium as carrier and buffer gas, entering the electrostatic time-of-flight mass-spectrometer through a 1 mm skimmer. To avoid detecting the comparably high amount of helium, the microchannel plate and phosphor screen detector voltages were gated. Because this gives a detector efficiency that gradually drops off for the lightest ions, we choose to present only ions with a mass/charge ratio of 25 u or greater.

3. Results and discussion

Results concerning three topics will be presented after an overview of adenine's main fragmentation channels in section 3.1. In section 3.2, we summarize our recent discovery of electronic dynamics that redistributes the charge and allows a stable dication to be produced. Thereafter, we examine the onset and decay times of several fragmentation channels in section 3.3 and finally the oscillations in two of them in section 3.4.
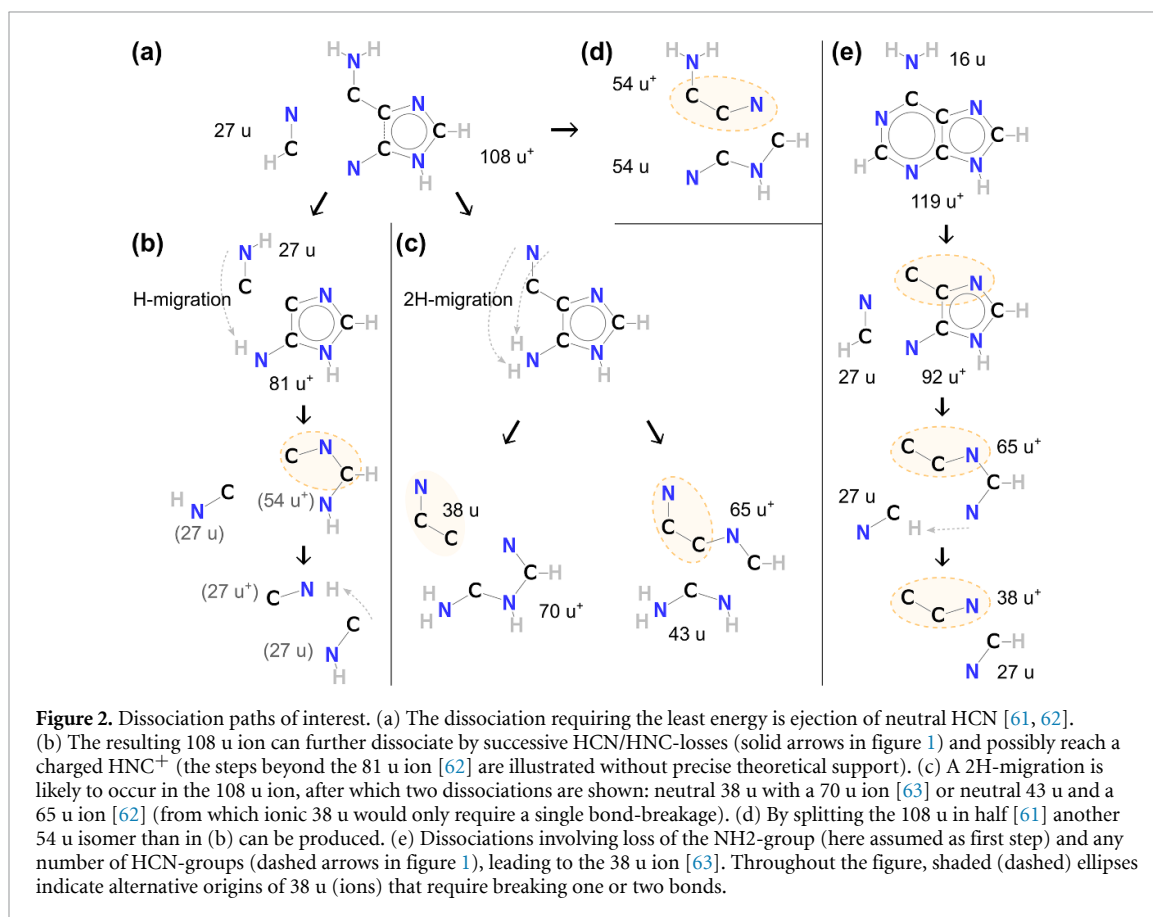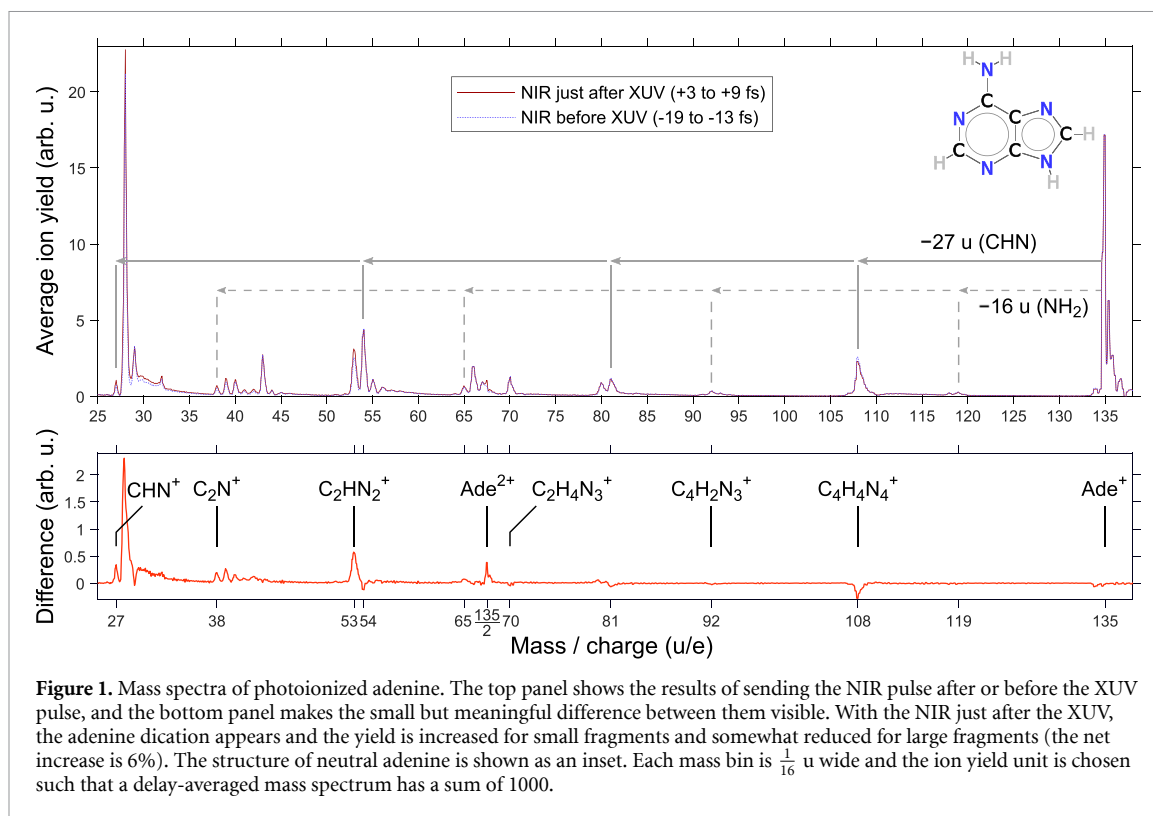
3.1. Pump–probe mass spectra

An overview of the mass spectra obtained when adenine (135 u, 8.20 eV ionization energy [63]) is photoionized by an XUV attosecond pulse, and probed by a NIR pulse is shown in figure 1. The ionic fragment with the lowest appearance energy is 108 u (11.3 to 12.3 eV [54, 63, 64]), via the loss of neutral 27 u as depicted in figure 2(a) [61–63, 65]. Adenine furthermore exhibits sequential ejection of neutral 27 u CHN-groups, indicated by solid arrows in figure 1. This gives rise to the fragments $C_nH_nN_n^+$ ($n = 5$ is the parent cation) with appearance energies increasing gradually to 14 ± 0.6 eV [54] for $n = 1$ (a charged 27 u CHN$^+$ fragment). CHN should be seen as a sum formula, referring to either of the HCN or HNC isomers, which are usually not distinguished. As exemplified in figures 2(a) and (b), some hydrogen migration is necessary for 81 u and 27 u ions, while (d) shows a shortcut to 54 u by ejecting $C_2H_2N_2$ in one step.

Dashed arrows in figure 1 indicate a sequence where also the neutral—NH$_2$ group is lost, explained in figure 2(e). This sequence ends with the 38 u C_2N^+ fragment whose relative yield varies considerably in the literature [6, 54, 64–66], most likely related to its higher appearance energy of 20–23 eV [54]. Simulations of 70 eV electron-impact-ionization [61] failed to reproduce both 38 u and 27 u ions, while they were stronger than the 39 u in an experiment using 14 keV projectiles [66]. While 38 u was seen for 3 keV Cl$^+$ projectiles, it was not for 6 keV F^{2+} [67] (and 27 u is not seen in any of their mass spectra next to the strong 28 u). In figures 2(b) and (e), the 27 and 38 u ions are assigned as the end products of long dissociation sequences, where small perturbations along the way might lead to other outcomes instead. In summary, the production of C_2N^+ can be significant under the right conditions (see e.g. [54, figure 7]) but difficult to reproduce in simulations, making it interesting to try to better understand the relevant kinetics by examining the ionization of adenine also with higher photon energies (above 22 eV [63]).

As is evident from figure 1, XUV-photoionization leads to a high level of fragmentation (81% of the total yield) regardless of when (and if) probed by the NIR-pulse, indicating the moderate photostability of adenine in the 17–35 eV energy range [54]. The dashed blue curve with the NIR pulse before the XUV has the same fragment distribution as the XUV gives on its own [6, supplementary information] but when the NIR pulse is sent after the XUV (solid red curve) it deposits further energy to the molecules ionized or highly excited by the XUV and helps to fragment them into smaller pieces. This is seen more clearly in the difference mass spectrum, as strong enhancements of many small ionic fragments and reduced yields of the larger fragments. The net change is positive, indicating that the NIR not only dissociates but also photoionizes. On its own, the NIR-pulse can produce parent cations through multi-photon ionization, but essentially without fragmentation (1% of the total yield was 108 u).

To extract physical information from a pump–probe experiment, we will use a curve model based on a differential equation system where the probed state is being populated via transitions with a total rate of $1/\tau_1$ and simultaneously decaying with a total rate of $1/\tau_2$ to non-observable states. Under the assumption that $0 \leqslant \tau_1 < \tau_2$, the solution has two exponential terms and can be analytically convoluted with a Gaussian to represent the finite pulse durations [6, supplementary information]. In the limiting case of $\tau_1 \approx 0$, the model simplifies to a step function that decays with lifetime τ_2, and represents probing from a state immediately populated by the short XUV-pulse. In the opposite case of probing a slowly populated final-state, which does
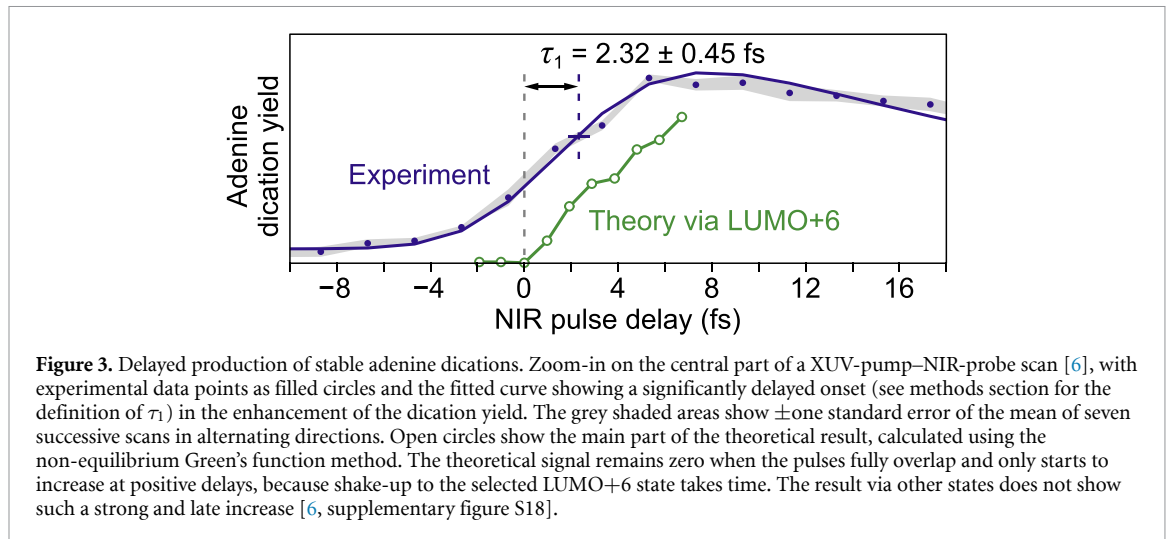
Figure 1. Mass spectra of photoionized adenine. The top panel shows the results of sending the NIR pulse after or before the XUV pulse, and the bottom panel makes the small but meaningful difference between them visible. With the NIR just after the XUV, the adenine dication appears and the yield is increased for small fragments and somewhat reduced for large fragments (the net increase is 6%). The structure of neutral adenine is shown as an inset. Each mass bin is $\frac{1}{16}$ u wide and the ion yield unit is chosen such that a delay-averaged mass spectrum has a sum of 1000.

Figure 2. Dissociation paths of interest. (a) The dissociation requiring the least energy is ejection of neutral HCN [61, 62]. (b) The resulting 108 u ion can further dissociate by successive HCN/HNC-losses (solid arrows in figure 1) and possibly reach a charged HNC$^+$ (the steps beyond the 81 u ion [62] are illustrated without precise theoretical support). (c) A 2H-migration is likely to occur in the 108 u ion, after which two dissociations are shown: neutral 38 u with a 70 u ion [63] or neutral 43 u and a 65 u ion [62] (from which ionic 38 u would only require a single bond-breakage). (d) By splitting the 108 u in half [61] another 54 u isomer than in (b) can be produced. (e) Dissociations involving loss of the NH2-group (here assumed as first step) and any number of HCN-groups (dashed arrows in figure 1), leading to the 38 u ion [63]. Throughout the figure, shaded (dashed) ellipses indicate alternative origins of 38 u (ions) that require breaking one or two bonds.

Figure 3. Delayed production of stable adenine dications. Zoom-in on the central part of a XUV-pump–NIR-probe scan [6], with experimental data points as filled circles and the fitted curve showing a significantly delayed onset (see methods section for the definition of τ_1) in the enhancement of the dication yield. The grey shaded areas show ±one standard error of the mean of seven successive scans in alternating directions. Open circles show the main part of the theoretical result, calculated using the non-equilibrium Green's function method. The theoretical signal remains zero when the pulses fully overlap and only starts to increase at positive delays, because shake-up to the selected LUMO+6 state takes time. The result via other states does not show such a strong and late increase [6, supplementary figure S18].

not decay within the scan range ($\tau_2 \to \infty$), the model can instead reduce to $(1 - e^{-t/\tau_1})h$. The step height h may be either positive or negative. Further details can be found in appendix A.

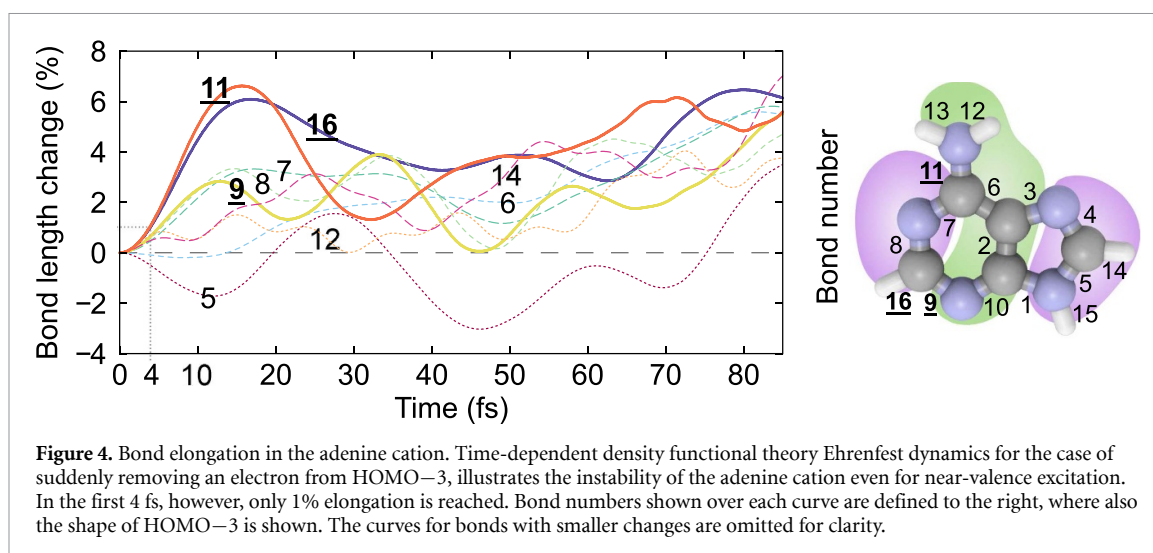### 3.2. Correlated electron dynamics in the adenine cation

In addition to the enhanced dissociation described in the previous section, we find that a delayed NIR-pulse also leads to the production of adenine^{2+}, the parent dication where no bond is broken but an extra electron is removed. Energetically, this outcome should be allowed already by the 17–35 eV XUV-pulse on its own, since, a dication appearance energy of 23.5 ± 1.0 eV is known from electron impact ionization [54]. However, we are not aware of any reports of adenine dications produced by photons, prior to our own [6].

The difference-spectrum in figure 1 shows that the dication with a mass/charge ratio of 135 u/2e = 67.5 u/e has the fourth strongest dependence on NIR-delay, and is much stronger than any other ion between 65 and 70 u/e. The existence of a 67 u ion from the XUV-photon alone, however, makes it difficult to determine the exact baseline level of adenine dications. An estimate, after adjusting for the partly overlapping peak shapes, is that the NIR-enhancement step height parameter, h, is $182 \pm 99\%$ of the baseline, which is more than twice as large as the relative enhancement for any fragment ion.

Even more interesting is that the dication enhancement starts, as seen in figure 3, with a small but certain delay compared to the changes in most of the cationic fragment yields, when fitting the pump–probe scans data as described in the Methods section. The zeroing of the delay-axis was described in the supplement of our previous publication [6]—briefly it is given by the simultaneous increase of many cationic fragments as well as atomic krypton (the Kr^{2+} yield). The onset-time for the dication is $\tau_1 = 2.32 \pm 0.45$ fs in the previously reported experiment (one fit to the average of seven successive delay-scans) [6]. Here we present the results obtained by including additional data from three other experiments performed on different days under similar conditions. With this procedure, we can now extract a new onset time of $\tau_1 = 2.42 \pm 0.80$ fs (median and sample standard deviation of fits to four experiments). τ_1 does not appear to depend on the NIR-intensity, although the enhancement most likely requires the absorption of two NIR photons (based on NIR-intensity scaling and the fitted Gaussian pulse widths) [6].

To investigate what mechanism can be responsible for the 2.4 fs delay between XUV-photoionization and the NIR-enhanced production of dications, we explored nuclear as well as electronic dynamics in different theoretical frameworks (see appendix B). First of all, we verified that even if an electron is only removed from any of the four highest occupied orbitals (lowest-energy holes), the instability of the adenine cation manifests itself as a substantial bond-elongation. The result with a hole in HOMO−3, as an example, is shown in figure 4, and several bonds oscillate and tend to elongate on a timescale of 15–85 fs (potentially proceeding toward dissociation). These calculations were made using time-dependent density functional theory (TDDFT) and Ehrenfest dynamics. We stress, however, that in the very beginning, it takes almost 4 fs before any bond has changed by 1%, so pure nuclear dynamics is not likely to be important for the observed phenomenon.

Considering instead the electronic dynamics, we identified that a multi-electronic process can fill the initial XUV-created inner-valence hole, while exciting at least one other electron to a normally unoccupied bound state. We refer to this as a *shake-up state* (although not requiring a shift in the kinetic energy of the primary photoelectron), but one can also refer to it as a frustrated Auger–Meitner-state (although no secondary electron has been emitted yet) [68, 69]. The cross-section for further photoionization by the
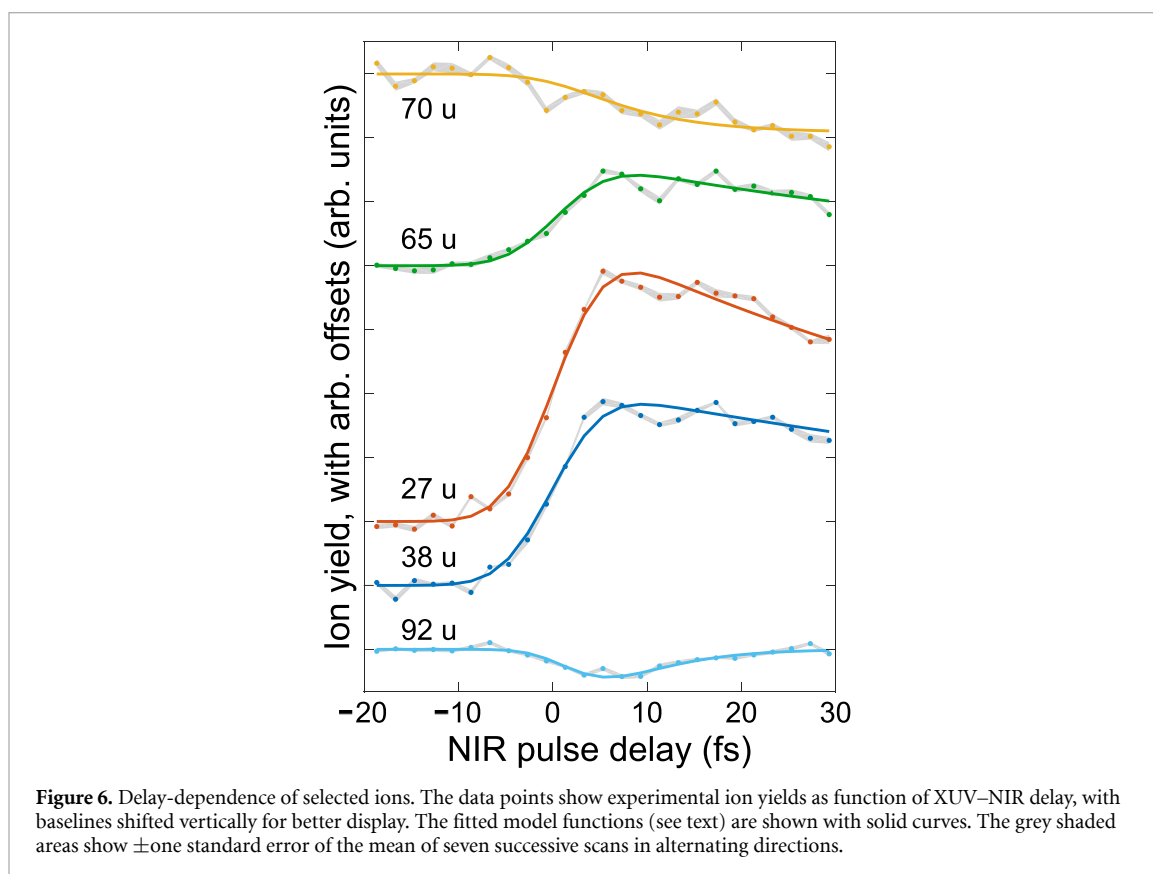
Figure 4. Bond elongation in the adenine cation. Time-dependent density functional theory Ehrenfest dynamics for the case of suddenly removing an electron from HOMO−3, illustrates the instability of the adenine cation even for near-valence excitation. In the first 4 fs, however, only 1% elongation is reached. Bond numbers shown over each curve are defined to the right, where also the shape of HOMO−3 is shown. The curves for bonds with smaller changes are omitted for clarity.
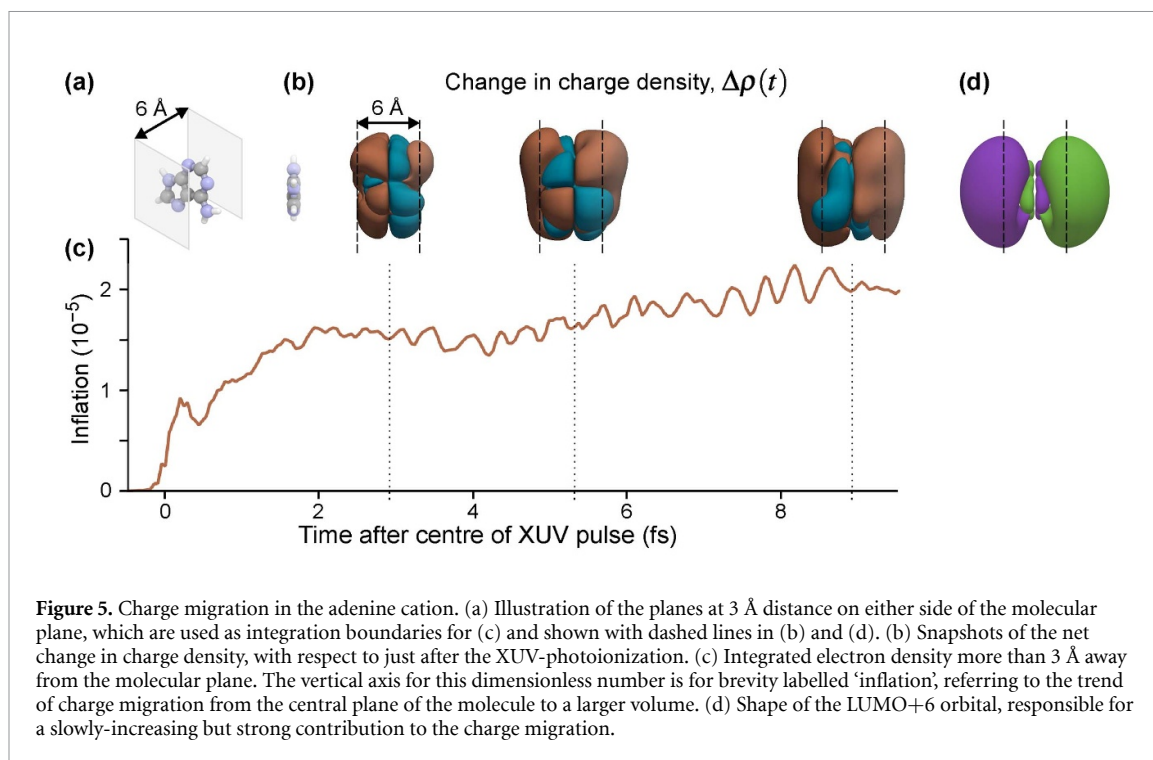
NIR-pulse would then vary depending on the shake-up state, favoring those with one highly excited electron whose ejection is allowed in a single-active-electron picture.

We examined this proposed mechanism using two complementary theoretical frameworks while keeping the nuclei fixed. A rate-based approach, consistent with the experimental curve model, used Fermi's golden rule and first-order perturbation theory to obtain exponential time-constants for each final-state of the highly excited electron. More sophisticated many-body time-dependent simulations were made using a method [6, 70, 71] based on the non-equilibrium Green's function that can handle both the shake-up electron dynamics triggered by the XUV photoionization and the subsequent absorption of a delayed NIR pulse. Both these methods singled out LUMO+6 as a unique shake-up state due to rising relatively slowly but surely, while being in the energy range favored by two-photon NIR-photoionization. The rate-equation approach gives a time-constant of about 3 fs for shake-up to LUMO+6 [6, figure 2]. The many-body-simulated XUV + NIR signal in figure 3 shows that the LUMO+6 contribution remains at zero when the pulses fully overlap (in contrast to an instantaneous transition which would have reached half of its peak-value) and then starts to grow nearly linearly with delay. After 4 fs it surpasses other states whose contributions stayed at a plateau reached within the first femtosecond [6, figure S18]. Even without discussing individual states of a particular basis set, the Green's function method allows visualization of the overall net change in electron density caused by intrinsic electronic relaxation: figure 5(b) shows snapshots with the change in electron density as function of time, with respect to just after XUV-ionization, visualized as red (increased) or blue (decreased). The electron density more than 3 Å from the plane of the molecule is integrated and shown as a curve in figure 5(c). It clearly grows with time. We label the vertical axis simply as 'inflation' to summarize that what this observable represents is a charge migration from the plane of the molecule to more than 3 Å outside. Although multiple states contribute, the importance of LUMO+6 is hinted by the fact that its orbital in panel (d) has large π-like lobes on either side of the molecular plane, like the net charge migration and intuitively a large electric-dipole transition matrix element for photoionization by the NIR-pulse.

To summarize, we deduced that a specific electronic rearrangement in inner-valence-ionized adenine opens up the possibility for the NIR-pulse to create stable dications of the intact molecule. Compared with any rapidly dissociating dications [72] that might be created by the XUV-pulse directly, the route involving shake-up and NIR-photoionization must be creating dications with less excitation energy, perhaps helped by ejecting the second photoelectron. While the NIR-pulse can immediately contribute to further dissociation of adenine cations, the stabilization-enabling process takes a relatively long time (τ_1 of a few femtoseconds) compared with other inner-valence electronic transitions, which makes this channel stand out in the experiment. The NIR-pulse then has to be sent before other processes, like the motion of the nuclei, close the window of opportunity—the dication signal decays with $\tau_2 = 22 \pm 4$ fs. However, if this sequence is completed, the resulting dication remains stable for at least the 3 μs it takes to traverse the mass spectrometer.

This combined theoretical and experimental work constitutes, to our knowledge, the first demonstration of *correlation-driven* charge migration. Conceptually, it is also more of a one-way charge migration than the back-and-forth oscillation so far observed in isolated amino acids [7, 39–41] and smaller systems [8, 9]. The mere ability to resolve a transition time of a few femtoseconds as non-instantaneous is testament to the usefulness of isolated attosecond pulses to investigate even molecules with as many as 15 atoms.

Figure 5. Charge migration in the adenine cation. (a) Illustration of the planes at 3 Å distance on either side of the molecular plane, which are used as integration boundaries for (c) and shown with dashed lines in (b) and (d). (b) Snapshots of the net change in charge density, with respect to just after the XUV-photoionization. (c) Integrated electron density more than 3 Å away from the molecular plane. The vertical axis for this dimensionless number is for brevity labelled 'inflation', referring to the trend of charge migration from the central plane of the molecule to a larger volume. (d) Shape of the LUMO+6 orbital, responsible for a slowly-increasing but strong contribution to the charge migration.

Figure 6. Delay-dependence of selected ions. The data points show experimental ion yields as function of XUV–NIR delay, with baselines shifted vertically for better display. The fitted model functions (see text) are shown with solid curves. The grey shaded areas show ±one standard error of the mean of seven successive scans in alternating directions.

3.3. Time constants for dissociation channels

While some fragment ion signals were already used as a time reference for accurate measurement of the *intact* dication's delay in [6], we here report a careful analysis of the time-constants extracted from the *dissociative* photoreactions, including data from many more ions. The delay-dependent yields of several fragments are shown in figure 6 and it is clear that they vary in different ways as a function of the XUV–NIR delay.

Starting with the τ_1-parameter that tells whether the probe's effect starts like a step function or gradually via a transition (defined on page 6), table 1 shows a clearly nonzero τ_1 for the 70 u cation $C_2H_4N_3^+$, in

Table 1. Summary of delay-dependence fitted for selected ions. The step height parameter expresses the enhancement (+) or suppression (−) with respect to the baseline signal at negative NIR-delay (approximately the XUV-only signal, but for 108 u and the parent cation the baseline also has a NIR-only contribution), before convolution with a Gaussian and not limited by the scan range. The table shows median values of fits to four experiments from different days with similar but not identical conditions, each containing 5, 6, 7 or 10 delay-scans. Uncertainties indicate the sample standard deviation between the four experiments and table cells with values smaller than their uncertainty are italicized. No time constants are shown for ions without clear delay-dependence (uncertain sign of the step height). For very long decay times, ∞ is shown rather than arbitrary values ($\geqslant 443$ fs) influenced by the chosen fitting bounds.

Mass (u)	Sum formula	τ_1 (fs)	τ_2 (fs)	Step height (arb. u.)	Relative step height (%)
27	CHN^+	0.5 ± 0.2	51 ± 10	$+1.8 \pm 0.8$	$+64 \pm 16$
38	C_2N^+	*0.6 ± 0.7*	56 ± 32	$+1.4 \pm 0.6$	$+48 \pm 28$
43	$CH_3N_2^+$	*0.9 ± 19*	∞	$+0.7 \pm 0.2$	$+5 \pm 3$
53	$C_2HN_2^+$	*0.7 ± 0.8*	63 ± 27	$+5.2 \pm 1.5$	$+30 \pm 9$
54	$C_2H_2N_2^+$	—	—	*-1.7 ± 2.4*	*-6 ± 9*
65	$C_3HN_2^+$	*0.4 ± 0.7*	42 ± 27	$+0.8 \pm 0.2$	$+17 \pm 9$
66	$C_3H_2N_2^+$	28 ± 17	∞	$+0.3 \pm 0.2$	$+3 \pm 2$
70	$C_2H_4N_3^+$	9.1 ± 5.1	*117 ± 326*	-0.5 ± 0.4	-10 ± 6
81	$C_3H_3N_3^+$	*3.0 ± 7.4*	∞	-0.7 ± 0.4	-9 ± 3
92	$C_4H_2N_3^+$	5.0 ± 3.3	7.0 ± 1.5	-0.5 ± 0.2	-16 ± 8
108	$C_4H_4N_4^+$	*0.4 ± 4.0*	47 ± 21	-2.6 ± 1.2	-13 ± 4
135	$C_5H_5N_5^{2+}$	2.4 ± 0.8	22 ± 4	$+2.2 \pm 1.2$	$(\approx +182 \pm 99)$
135	$C_5H_5N_5^+$	—	—	*-2.4 ± 3.4*	*-3 ± 4*

addition to the previously described 2.4 fs electronic dynamics leading to the dication. The 70 u ion yield is hardly influenced by the NIR-probe at zero delay in figure 6 but is then gradually depleted, with the time constant $\tau_1 = 9.1 \pm 5.1$ fs. The uncertainty mainly represents the possibility of a continued slope outside the scan range and an even longer τ_1 (the four experiments summarized in table 1 gave τ_1 from 8.7 to 19.2 fs), while a shorter τ_1 would fail to fit the data. The 70 u fragment is one of the few that require a concerted two-hydrogen migration [63], which turns the 108 u precursor ion into its lowest-energy isomer [62] and enables the dissociation path shown in figure 2(c). We can therefore speculate that the XUV-ionized molecule evolves in a way that eventually allows the NIR-absorption to suppress fragmentation into 70 u by preventing the initial hydrogen migration.
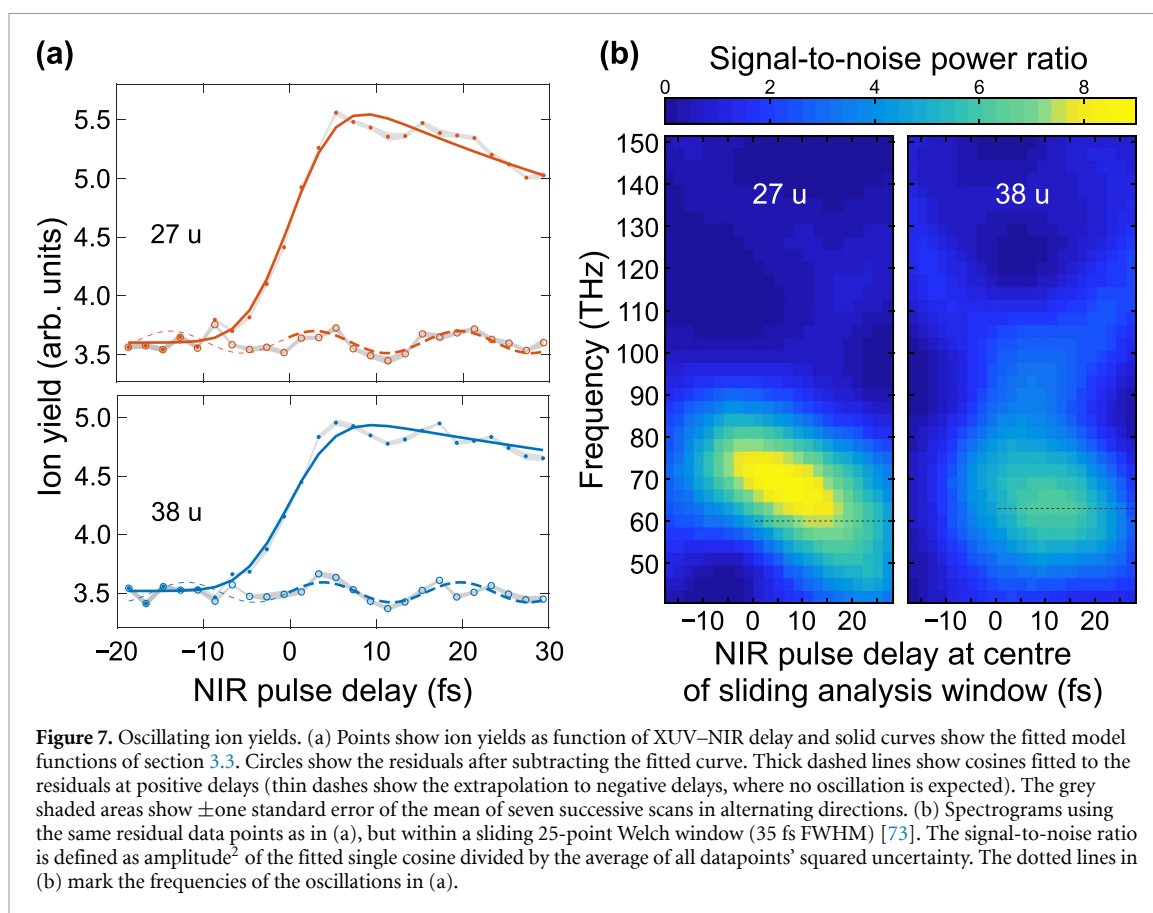
The lifetime τ_2 tells how quickly the effect of the NIR-probe decays or recovers, and values between 40 and 70 fs are found for many of the fragment ions in table 1. Shorter lifetimes are found for the dication (22 ± 4 fs) and for the weak dip in the 92 u yield (7.0 ± 1.5 fs).

The fragment ions most strongly affected by the NIR-probe are 53 u, 108 u, 27 u and 38 u (all shown in [6]). We will here focus on 27 and 38 u, which have the largest relative step heights: 64% and 48% of their negative-delay (or XUV-only) baselines, and whose relative yield has varied between types of experiments in the literature (see section 3.1). In the following section we will also examine possible oscillations in their fragment yields.

Neutral 27 u HCN or HNC fragments appear in many dissociation paths of adenine (e.g. 40% of those in [64]), with several examples shown in figure 2 based on assignments for ionization by a single photon or projectile. It is, however, not clear which dissociation path is the most likely to yield *charged* 27 u fragments for one-photon ionization and whether the delayed NIR probe enhances the same or another path. Since the 38 u ion has been investigated less in the previous literature, we drew ellipses in figure 2 to mark where C_2N could be produced in other ways than via the known—NH_2-loss sequence in figure 2(e) [63]. We then included the suggested precursors or competing products in table 1 to look for similarities in delay-dependence. Seeing that the 54 u yield is not influenced by the probe-pulse allows us to exclude figures 2(b) and (d), and that the time constants for 70 u and 43 u are very different from those for 38 u speaks against figure 2(c). We thus conclude that 65 u is the most plausible precursor for 38 u, and it is remarkable that the complementary part of 65 u would be 27 u, i.e. 65 u could be a precursor for *both* of the fragments with the largest relative NIR-enhancement. Different isomers of 65 u appear in the (c) and (e) dissociation paths, in both cases with the breakage of a CN-bond as a final step.

3.4. Oscillating fragment yields

To examine whether there is any oscillation in the ion yields on top of the time dependence fitted in the previous section, a single-frequency oscillation was fitted to the residual data points, using only the part of the scan at positive NIR delay to select oscillations excited by the XUV-ionization. Such oscillations are found for the 27 u HCN^+/HNC^+ and 38 u C_2N^+ fragment yields, as shown by dashed lines in figure 7(a). The median and standard deviations for the periods in four experiments under similar conditions are 15.0 ± 3.2 fs and 17.2 ± 3.8 fs, respectively. Oscillation periods for the other ions were not consistent between experiments,

Figure 7. Oscillating ion yields. (a) Points show ion yields as function of XUV–NIR delay and solid curves show the fitted model functions of section 3.3. Circles show the residuals after subtracting the fitted curve. Thick dashed lines show cosines fitted to the residuals at positive delays (thin dashes show the extrapolation to negative delays, where no oscillation is expected). The grey shaded areas show ±one standard error of the mean of seven successive scans in alternating directions. (b) Spectrograms using the same residual data points as in (a), but within a sliding 25-point Welch window (35 fs FWHM) [73]. The signal-to-noise ratio is defined as amplitude^2 of the fitted single cosine divided by the average of all datapoints' squared uncertainty. The dotted lines in (b) mark the frequencies of the oscillations in (a).

with standard deviations of 6–7 fs for two of them and exceeding 11 fs for eight of them. The 27 u and 38 u oscillations have similar periods and are initiated with approximately the same phase, having the first cosine peak at NIR-delays of 5 ± 4 and 6 ± 4 fs. This suggests that the modulating NIR-transition occurs as a common precursor rather than as a delay-dependent competition between the two fragmentation outcomes.

To investigate whether the oscillation frequency or amplitude vary during the scan, figure 7(b) shows spectrograms computed using a sliding Welch [73] window function. Its spectral properties lie between those of the Hann and the rectangular windows [74]. We find that the oscillations are stronger when the window is centered near the end of the scan (e.g., +25 fs) than when close to the start of the scan (e.g. −15 fs), which confirms that the oscillations occur in the XUV-ionized sample and are probed by the NIR-pulse (not excited by the NIR-pulse). The strongest signal/noise ratio is found at NIR-delays of 5–10 fs, near the peaks of the non-oscillating model curves in figure 7(a).

In the frequency range of the observed oscillation, neither coherent beating between electronic states nor coherently excited vibrational wavepackets can be excluded *a priori*. The onset of nuclear motion could change the spacing between electronic states and lead to decoherence [75, 76] but the oscillation amplitude remains roughly constant for at least as long as the τ_2 lifetime of the non-oscillating step. While a time-dependent localization of charge on the 27 u-side in the dissociation figure 2(a) could probably modulate the 27 u ion yield, there does not appear to be any such immediate path toward charged 38 u fragments. Considering these arguments and the difficulty of simulating coherent electronic dynamics while letting the nuclei move, we will in the following focus on a vibrational assignment.

The observed oscillation frequency is consistent with the general band for CN-stretching vibrations, possibly in the 65 u precursor and certainly in the neutral 27 u and 38 u fragments (16 fs for HN–C [77] and HC–N [78], 17 fs for C–C–N asymmetric stretch [79, 80]). Although NIR-photoionization of electronically excited fragments can have a cross-section dependent on their bond lengths, such an assignment is difficult to reconcile with the immediate onset of the oscillations. In particular, the 38 u fragment shown in figure 2 cannot be formed without substantial nuclear motion [61, 63], which must be expected to take time.

To get an idea of which bonds start to elongate *quickly*, and better support a vibrational explanation, we revisit figure 4 and our TDDFT Ehrenfest dynamics calculations for the adenine cation [6, supplementary figure S10]. Two CN-bonds in the backbone show rapid elongation: bond #9 relating to figure 2(a) and bond #11 which concerns the—NH$_2$-group which has already been highlighted in the dissociation path of figure 2(e). Figure 4 shows that the C–NH$_2$ bond #11 elongates dramatically by 6.5% in 15 fs after the sudden

removal of an electron from HOMO-3. The simulation as well as vibronic spectroscopy on adenine [81, 82] give period times of 30–33 fs for this bond, so that its second overtone would match the ion yield oscillations perfectly. A coherent comb beating at twice the fundamental frequency could be excited if only the even-numbered vibrational levels have nonzero Franck–Condon factors [83] (or classically by a transition occurring only at the equilibrium geometry twice per oscillation period). Within the experimental uncertainty, a directly matching fundamental 20 fs oscillation period has also been reported for a mode that involves both the C–NH$_2$ stretch and NH$_2$ scissoring [84–86]. (An even better matching peak at 17 fs, 1909 cm^{-1}, in the calculations of Nowak *et al* [86] was weak and not assigned.)

4. Conclusions

Controlling photochemical reactions requires a thorough understanding of both electronic and vibrational dynamics. The greatest challenges for theoretical work can be found at ultrafast time scales, in energy-ranges where electronic correlation is important (inner-valence holes) and with large molecules. In this work, we time-resolved different types of relaxation processes in the nucleobase adenine (C$_5$H$_5$N$_5$) after photoionization in the previously unexplored XUV energy range, also relevant for DNA-damage by secondary electrons in tissue.

Our XUV-pump—NIR-probe experiment provides onset- and decay-times of molecular processes which are revealed by how the yields of the intact adenine dication and several fragment ions are influenced by the NIR pulse at different time delays. Using this approach, we have been able to extract decay times for the 65, 66, 70 and 92 u channels (never reported before) and refine values for the recently reported stronger channels. Although the precise non-adiabatic mechanisms responsible for their decays have not been elucidated, assignments were given for the few-femtosecond delayed onsets discovered for the 70 u C$_2$H$_4$N$_3^+$ fragment ion and the dication (C$_5$H$_5$N$_5^{2+}$). The former may be related to double hydrogen-migration that is required to form C$_2$H$_4$N$_3^+$. The latter was assigned as a kind of charge migration with the help of first-principles theory and represents the first time that a multi-electronic process in a polyatomic molecule has been tracked in real time [6]. The time required for the charge migration allowed us to achieve a degree of control of the yield of intact dications via the XUV–NIR delay parameter and the ability to resolve the phenomenon as non-instantaneous demonstrates the potential of attosecond technology even for molecules with as many as 15 atoms.

Furthermore, we propose that delay-dependent oscillations in the yields of the 27 u CHN$^+$ and 38 u C$_2$N$^+$ fragment ions may be a consequence of C–NH$_2$-stretching vibrations in the adenine cation. The XUV attosecond pulse excites a broadband coherent vibrational wave packet whose beating, as a function of delay before the NIR-probe is absorbed, may modulate the probability of entering the dissociation path in figure 2(e) where loss of NH$_2$ is necessary. The similar oscillation amplitudes for HCN$^+$ and C$_2$N$^+$ suggest that a similar number of steps are required, i.e., that the oscillating HCN$^+$ is formed after hydrogen migration together with a neutral 65 or 38 u, rather than directly with 92 u. The multi-step dissociation paths that can lead to 27 or 38 u ions have not received much attention in previous studies (particularly with the C$_2$N$^+$ branching ratio varying substantially between different ionization methods and between experiment and theory), and our findings provide new insights toward the understanding of vibrational wave packet dynamics of this relatively large molecule.

In summary, by controlling when the NIR-pulse is sent with extreme time resolution we have been able to suppress and enhance different molecular dissociation channels, both in a conventional way by exploiting vibronic dynamics and in a novel way based on pure electronic dynamics. Further advances in the ability to control photochemistry at its natural timescale [10, 12] may come from the development of more advanced simulations for polyatomic systems going beyond the Born-Oppenheimer approximation and by combining them with experimental investigations, such as the present one, which covers the full range from electronic, vibrational to dissociative phenomena.

Data availability statement

The data that support the findings of this study are available from the corresponding author upon reasonable request.

Acknowledgments

Appendix A. Fitting and statistics

For each experiment, ion yields from multiple delay-scans are averaged and errorbars defined by the standard error of the mean. The curve model introduced on page 6 is expanded for a global fit of the delay-dependent signals for all the analysed ions, where the pulse duration is a shared parameter and each ion has individual parameters for baseline, step height, exponential onset-time τ_1 and exponential decay-time τ_2.

The Gaussian for each signal has a full-width at half-max $W/\sqrt{n_i}$ where W represents NIR pulse duration and n_i is the number of NIR-photons absorbed for the signal of ion i (usually 1 but chosen as 2 for 92 u, 108 u and the adenine dication). The zeroing of the delay-axis can be fitted as an additional common parameter but for the main experiment it is held fixed to agree exactly with our previous publication [6] (would otherwise vary on the 0.1 fs level depending on which ions are included in the global fit). Additionally, we have here considered three similar experiments to check the robustness and provide median-values and sample standard deviations of fitted parameters.

For oscillations fitted to residuals beyond the above curve model, significance can be judged via the signal-to-noise power ratio (computed as the fitted cosine's squared amplitude divided by the average of all datapoints' squared signal-errorbars). Its statistical distribution is known for the null hypothesis of no real signal, so for a p-value of 5% a signal-to-noise ratio of 6.6 is considered significant, including the correction [87] for examining multiple frequencies (37 here, in steps of 3 THz from 42 to 150 THz). Additionally, we compute the difference in corrected Akaike Information Criterion (dAICc) [88] with the sign chosen to be positive if the cosine model function is preferred over a single-parameter constant model. The residual oscillations in figure 7(a) for 27 u and 38 u have the respective signal-to-noise ratios 7.7 and 7.5 (corresponding to p-values of 0.017 and 0.020) and dAICc-values of 4.7 and 8.4.

Appendix B. Theory

In this section we describe the basics of the theoretical approaches employed to simulate the photo-induced nuclear and electronic dynamics in adenine.

B.1. Nuclear dynamics
TDDFT, the extension to the time-domain of the ordinary density functional theory is a formally exact quantum mechanical *ab-initio* method able to describe the dynamics of many-body systems [89, 90]. The TDDFT standpoint is the effective one-particle potential called exchange-correlation potential. While TDDFT within standard exchange-correlation functionals flavours is not able to capture the level of electronic correlation required to describe the correct correlated electronic dynamics in ionized adenine, it can still be used as an affordable solution to simulate the qualitative dynamical nuclear behavior following XUV ionization. Specifically, we follow the nuclear motion after a sudden single (or double) ionization by means of TDDFT + Ehrenfest dynamics within a self-interaction-corrected PBE exchange correlation functional [91, 92]. The TDDFT + Ehrenfest dynamics method is a non-adiabatic molecular dynamics approach which couples the time-dependent propagation of the Kohn–Sham orbitals with classical equations of motion for the nuclei determined on the base of the electronic potential energy surface (PES). In practice, the combined electronic–nuclear dynamics is carried out by a time stepping procedure where first the electronic evolution is obtained from TDDFT to calculate the time-evolved density and the latter is then used to calculate the PES from which the nuclear forces are evaluated and used to displace the nuclei within classical equations of motion. While this approach allows to treat non-adiabatic effects, it is formally justified

only as long as the nuclear propagation is well described by single PESs and no quantum mixing of nuclear trajectories is expected to take place, like in the case of conical intersections which we neglect in this work. We utilize the Octopus code [93, 94] to perform TDDFT + Ehrenfest dynamics on adenine following the single (or double) removal of an electron from a given Kohn–Sham state. As discussed in the text we are able to demonstrate that ionization of adenine without any stabilization mechanism initiated by electronic correlation inevitably leads to bond elongation (figure 4) and eventual molecular dissociation on a time scale (>10 fs) much longer than the one associated with the electronic charge migration.

B.2. Correlated electronic dynamics

As mentioned in the above section the available TDDFT exchange correlation potentials are not mature enough to capture the electronic correlation necessary to describe shake-up effects. For this reason we here employ a time-dependent density matrix propagation method based on non-equilibrium Green's function theory (NEGF) [95]. The NEGF formalism is based on a non-local non-hermitian self-energy operator comparable to the exchange-correlation potential in TDDFT, with the fundamental difference that one has a systematic perturbative approach to handle electron-electron and electron-photon interactions. The time-dependent equation for the density matrix reads:

$$\frac{d}{dt}\hat{\rho}(t) + i\left[\hat{h}_{\mathrm{HF}}(t), \hat{\rho}(t)\right] = -\hat{I}_{\mathrm{c}}(t) - \hat{I}_{\mathrm{c}}^{\dagger}(t) - \hat{I}_{\mathrm{ion}}(t) - \hat{I}_{\mathrm{ion}}^{\dagger}(t),$$

where $\hat{h}_{\mathrm{HF}}(t)$ is the single particle Hartree–Fock Hamiltonian describing the system, and $\hat{I}_{\mathrm{c}}(t)$ and $\hat{I}_{\mathrm{ion}}(t)$ are the collision and ionization integrals respectively. The collision integral, which is expressed in terms of the correlation self-energy contains all the relevant electron-electron scattering processes. The ionization integral instead allows to include the laser induced ionization. Recent implementations of the density matrix propagation approach, such as the one in the CHEERS code [70], have made accurate simulations of realistic systems computationally accessible. Here we numerically solve the above equation for the charge dynamics of adenine induced by an experimental attosecond XUV pulse. Specifically, we construct the Hartree–Fock Hamiltonian starting from the Kohn–Sham wavefunctions and approximate the self-energy at the second-Born level; all details are provided in our recent report [6].

ORCID iDs

Erik P Månsson ⬤ https://orcid.org/0000-0003-3567-2985
Vincent Wanie ⬤ https://orcid.org/0000-0001-8274-4617
Gianluca Stefanucci ⬤ https://orcid.org/0000-0001-6197-8043
Umberto De Giovannini ⬤ https://orcid.org/0000-0002-4899-1304
Andrea Trabattoni ⬤ https://orcid.org/0000-0002-0187-9075
Fabio Frassetto ⬤ https://orcid.org/0000-0001-5528-1995
Jason B Greenwood ⬤ https://orcid.org/0000-0001-9470-7223
Mauro Nisoli ⬤ https://orcid.org/0000-0003-2309-732X

References

[1] Zewail A H 2000 Femtochemistry: atomic-scale dynamics of the chemical bond using ultrafast lasers (Nobel lecture) *Angew. Chem., Int. Ed.* **39** 2586–631
[2] Gruebele M and Zewail A H 1993 Femtosecond wave packet spectroscopy: coherences, the potential and structural determination *J. Chem. Phys.* **98** 883–902
[3] Drescher M, Hentschel M, Kienberger R, Uiberacker M, Yakovlev V, Scrinzi A, Westerwalbesloh T, Kleineberg U, Heinzmann U and Krausz F 2002 Time-resolved atomic inner-shell spectroscopy *Nature* **419** 803–7
[4] Hanna A M, Vendrell O, Ourmazd A and Santra R 2017 Laser control over the ultrafast Coulomb explosion of N_2^{2+} after Auger decay: a quantum-dynamics investigation *Phys. Rev.* A **95** 043419
[5] Uiberacker M *et al* 2007 Attosecond real-time observation of electron tunnelling in atoms *Nature* **446** 627–32
[6] Månsson E P *et al* 2021 Real-time observation of a correlation-driven sub 3 fs charge migration in ionised adenine *Commun. Chem.* **4** 73
[7] Calegari F *et al* 2014 Ultrafast electron dynamics in phenylalanine initiated by attosecond pulses *Science* **346** 336–9
[8] Ranitovic P *et al* 2014 Attosecond vacuum UV coherent control of molecular dynamics *Proc. Natl Acad. Sci.* **111** 912–7
[9] Kraus P M *et al* 2015 Measurement and laser control of attosecond charge migration in ionized iodoacetylene *Science* **350** 790–5
[10] Palacios A and Martín F 2019 The quantum chemistry of attosecond molecular science *WIREs Comput. Mol. Sci.* **10** e1430
[11] Kraus P M and Wörner H J 2018 Perspectives of attosecond spectroscopy for the understanding of fundamental electron correlations *Angew. Chem., Int. Ed.* **57** 5228–47
[12] Lépine F, Ivanov M Y and Vrakking M J J 2014 Attosecond molecular dynamics: fact or fiction? *Nat. Photon.* **8** 195–204
[13] Young L *et al* 2018 Roadmap of ultrafast x-ray atomic and molecular physics *J. Phys. B: At. Mol. Opt. Phys.* **51** 032003
[14] Lewenstein M, Balcou P, Ivanov M Y, L'Huillier A and Corkum P B 1994 Theory of high-harmonic generation by low-frequency laser fields *Phys. Rev.* A **49** 2117–32

[15] Nisoli M, Decleva P, Calegari F, Palacios A and Martín F 2017 Attosecond electron dynamics in molecules *Chem. Rev.* **117** 10760–825

[16] Hentschel M, Kienberger R, Spielmann C, Reider G A, Milosevic N, Brabec T, Corkum P, Heinzmann U, Drescher M and Krausz F 2001 Attosecond metrology *Nature* **414** 509–13

[17] Itatani J, Quéré F, Yudin G L, Yu M Krausz I, F and Corkum P B 2002 Attosecond streak camera *Phys. Rev. Lett.* **88** 173903

[18] Muller H G 2002 Reconstruction of attosecond harmonic beating by interference of two-photon transitions *Appl. Phys.* B **74** s17–s21

[19] Dahlström J M, L'Huillier A and Maquet A 2012 Introduction to attosecond delays in photoionization *J. Phys. B: At. Mol. Opt. Phys.* **45** 183001

[20] Ossiander M *et al* 2016 Attosecond correlation dynamics *Nat. Phys.* **13** 280–5

[21] Cirelli C *et al* 2018 Anisotropic photoemission time delays close to a Fano resonance *Nat. Commun.* **9** 955

[22] Månsson E P *et al* 2014 Double ionization probed on the attosecond timescale *Nat. Phys.* **10** 207–11

[23] Cattaneo L, Vos J, Bello R Y, Palacios A, Heuser S, Pedrelli L, Lucchini M, Cirelli C, Martín F and Keller U 2018 Attosecond coupled electron and nuclear dynamics in dissociative ionization of H_2 *Nat. Phys.* **14** 733–8

[24] Nandi S *et al* 2020 Attosecond timing of electron emission from a molecular shape resonance *Sci. Adv.* **6** eaba7762

[25] Jordan I, Huppert M, Rattenbacher D, Peper M, Jelovina D, Perry C, von Conta A, Schild A and Wörner H J 2020 Attosecond spectroscopy of liquid water *Science* **369** 974–9

[26] Quan W, Serov V V, Wei M, Zhao M, Zhou Y, Wang Y, Lai X, Kheifets A S and Liu X 2019 Attosecond molecular angular streaking with all-ionic fragments detection *Phys. Rev. Lett.* **123** 223204

[27] Fuchs J, Douguet N, Donsa S, Martin F, Burgdörfer J, Argenti L, Cattaneo L and Keller U 2020 Time delays from one-photon transitions in the continuum *Optica* **7** 154

[28] Geneaux R, Marroux H J B, Guggenmos A, Neumark D M and Leone S R 2019 Transient absorption spectroscopy using high harmonic generation: a review of ultrafast x-ray dynamics in molecules and solids *Phil. Trans. R. Soc.* A **377** 20170463

[29] Berera R, van Grondelle R and Kennis J T M 2009 Ultrafast transient absorption spectroscopy: principles and application to photosynthetic systems *Photosynth. Res.* **101** 105–18

[30] Grégoire G, Kang H, Dedonder-Lardeux C, Jouvet C, Desfrançois C, Onidas D, Lepere V and Fayeton J A 2006 Statistical vs. non-statistical deactivation pathways in the UV photo-fragmentation of protonated tryptophan–leucinedipeptide *Phys. Chem. Chem. Phys.* **8** 122–8

[31] Erk B *et al* 2014 Imaging charge transfer in iodomethane upon x-ray photoabsorption *Science* **345** 288–91

[32] Hervé M, Boyer A, Brédy R, Compagnon I, Allouche A-R and Lépine F 2021 Controlled ultrafast $\pi\pi^*$–$\pi\sigma^*$ dynamics in tryptophan-based peptides with tailored micro-environment *Commun. Chem.* **4** 124

[33] Zettergren H *et al* 2021 Roadmap on dynamics of molecules and clusters in the gas phase *Eur. Phys. J.* D **75** 152

[34] Cederbaum L S and Zobeley J 1999 Ultrafast charge migration by electron correlation *Chem. Phys. Lett.* **307** 205–10

[35] Wörner H J *et al* 2017 Charge migration and charge transfer in molecular systems *Struct. Dyn.* **4** 061508

[36] Weinkauf R, Schanen P, Metsala A, Schlag E W, Bürgle M and Kessler H 1996 Highly efficient charge transfer in peptide cations in the gas phase: threshold effects and mechanism *J. Phys. Chem.* **100** 18567–85

[37] Kuleff A I and Cederbaum L S 2014 Ultrafast correlation-driven electron dynamics *J. Phys. B: At. Mol. Opt. Phys.* **47** 124002

[38] Remacle F and Levine R D 2006 An electronic time scale in chemistry *Proc. Natl Acad. Sci.* **103** 6793–8

[39] Trabattoni A, Galli M, Lara-Astiaso M, Palacios A, Greenwood J, Tavernelli I, Decleva P, Nisoli M, Martín F and Calegari F 2019 Charge migration in photo-ionized aromatic amino acids *Phil. Trans. R. Soc.* A **377** 20170472

[40] Lara-Astiaso M *et al* 2018 Attosecond pump–probe spectroscopy of charge dynamics in tryptophan *J. Phys. Chem. Lett.* **9** 4570–7

[41] Lara-Astiaso M, Palacios A, Decleva P, Tavernelli I and Martín F 2017 Role of electron-nuclear coupled dynamics on charge migration induced by attosecond pulses in glycine *Chem. Phys. Lett.* **683** 357–64

[42] Khalili F, Vafaee M and Shokri B 2021 Attosecond charge migration following oxygen K-shell ionization in DNA bases and base pairs *Phys. Chem. Chem. Phys.* **23** 23005–13

[43] Huels M A, Boudaïffa B, Cloutier P, Hunting D and Sanche L 2003 Single, double and multiple double strand breaks induced in DNA by 3–100 eV electrons *J. Am. Chem. Soc.* **125** 4467–77

[44] Jahnke T *et al* 2010 Ultrafast energy transfer between water molecules *Nat. Phys.* **6** 139–42

[45] Mucke M, Braune M, Barth S, Förstel M, Lischke T, Ulrich V, Arion T, Becker U, Bradshaw A and Hergenhahn U 2010 A hitherto unrecognized source of low-energy electrons in water *Nat. Phys.* **6** 143–6

[46] Kuhlmann A, Bihr L and Wagenknecht H-A 2020 How far does energy migrate in DNA and cause damage? evidence for long-range photodamage to DNA *Angew. Chem., Int. Ed.* **59** 17378–82

[47] Ullrich S, Schultz T, Zgierski M Z and Stolow A 2004 Electronic relaxation dynamics in DNA and RNA bases studied by time-resolved photoelectron spectroscopy *Phys. Chem. Chem. Phys.* **6** 2796

[48] Canuel Clelia, Mons M, Piuzzi F, Tardivel B, Dimicoli I and Elhanine M 2005 Excited states dynamics of DNA and RNA bases: characterization of a stepwise deactivation pathway in the gas phase *J. Chem. Phys.* **122** 074316

[49] Gustavsson T, Improta R and Markovitsi D 2010 DNA/RNA: building blocks of life under UV irradiation *J. Phys. Chem. Lett.* **1** 2025–30

[50] Yu H, Sanchez-Rodriguez J A, Pollum M, Crespo-Hernández C E, Mai S, Marquetand P, González L and Ullrich S 2016 Internal conversion and intersystem crossing pathways in UV excited, isolated uracils and their implications in prebiotic chemistry *Phys. Chem. Chem. Phys.* **18** 20168–76

[51] Williams H L, Erickson B A and Neumark D M 2018 Time-resolved photoelectron spectroscopy of adenosine and adenosine monophosphate photodeactivation dynamics in water microjets *J. Chem. Phys.* **148** 194303

[52] Muñoz A, Oller J C, Blanco F, Gorfinkiel J D, Limão-Vieira P and García G 2007 Electron-scattering cross sections and stopping powers in H_2O *Phys. Rev.* A **76** 052707

[53] Månsson E P, De Camillis S, Castrovilli M C, Galli M, Nisoli M, Calegari F and Greenwood J B 2017 Ultrafast dynamics in the DNA building blocks thymidine and thymine initiated by ionizing radiation *Phys. Chem. Chem. Phys.* **19** 19815–21

[54] van der Burgt P J M, Finnegan S and Eden S 2015 Electron impact fragmentation of adenine: partial ionization cross sections for positive fragments *Eur. Phys. J.* D **69** 173

[55] Nisoli M, De Silvestri S and Svelto O 1996 Generation of high energy 10 fs pulses by a new pulse compression technique *Appl. Phys. Lett.* **68** 2793–5

[56] Nisoli M, De Silvestri S, Svelto O, Szipöcs R, Ferencz K, Spielmann C, Sartania S and Krausz F 1997 Compression of high-energy laser pulses below 5 fs *Opt. Lett.* **22** 522

[57] Sola I J *et al* 2006 Controlling attosecond electron dynamics by phase-stabilized polarization gating *Nat. Phys.* **2** 319–22

[58] Sansone G *et al* 2006 Isolated single-cycle attosecond pulses *Science* **314** 443–6

[59] Calegari F, Sansone G, Stagira S, Vozzi C and Nisoli M 2016 Advances in attosecond science *J. Phys. B: At. Mol. Opt. Phys.* **49** 062001

[60] López-Martens R *et al* 2005 Amplitude and phase control of attosecond light pulses *Phys. Rev. Lett.* **94** 033001

[61] Bauer C A and Grimme S 2014 Elucidation of electron ionization induced fragmentations of adenine by semiempirical and density functional molecular dynamics *J. Phys. Chem.* A **118** 11479–84

[62] Minaev B F, Shafranyosh M I, Svida Y Y, Sukhoviya M I, Shafranyosh I I, Baryshnikov G V and Minaeva V A 2014 Fragmentation of the adenine and guanine molecules induced by electron collisions *J. Chem. Phys.* **140** 175101

[63] Jochims H-W, Schwell M, Baumgärtel H and Leach S 2005 Photoion mass spectrometry of adenine, thymine and uracil in the 6–22eV photon energy range *Chem. Phys.* **314** 263–82

[64] Pilling S, Lago A F, Coutinho L H, de Castilho R B, de Souza G G B and de Brito A N 2007 Dissociative photoionization of adenine following valence excitation *Rapid Commun. Mass Spectrom.* **21** 3646–52

[65] Rice J M and Dudek G O 1967 Mass spectra of nucleic acid derivatives. II. Guanine, adenine and related compounds *J. Am. Chem. Soc.* **89** 2719–25

[66] Alvarado F, Bari S, Hoekstra R and Schlathölter T 2007 Interactions of neutral and singly charged keV atomic particles with gas-phase adenine molecules *J. Chem. Phys.* **127** 034301

[67] Brédy R, Bernard Jême, Chen Li, Montagne G, Li B and Martin S 2009 Fragmentation of adenine under energy control *J. Chem. Phys.* **130** 114305

[68] Bagus P S, Broer R and Ilton E S 2004 A new near degeneracy effect for photoemission in transition metals *Chem. Phys. Lett.* **394** 150–4

[69] Despré V and Kuleff A I 2021 Correlation-driven charge migration as initial step in the dynamics in correlation bands (arXiv:2111.00760)

[70] Perfetto E and Stefanucci G 2018 CHEERS: a tool for correlated hole-electron evolution from real-time simulations *J. Phys.: Condens. Matter* **30** 465901

[71] Covito F, Perfetto E, Rubio A and Stefanucci G 2018 Real-time dynamics of Auger wave packets and decays in ultrafast charge migration processes *Phys. Rev. A* **97** 061401

[72] Moretto-Capelle P, Le Padellec A, Brière G, Massou S and Franceries Fèric 2007 Energetics and metastability of the adenine dication observed in proton-adenine collisions *J. Chem. Phys.* **127** 234311

[73] Welch P 1967 The use of fast Fourier transform for the estimation of power spectra: a method based on time averaging over short, modified periodograms *IEEE Trans. Audio Electroacoust.* **15** 70–73

[74] Heinzel G, Rüdiger A and Schilling R 2002 Spectrum and spectral density estimation by the discrete fourier transform (DFT), including a comprehensive list of window functions and some new at-top windows *Technical Report* (Laser Interferometry & Gravitational Wave Astronomy, AEI-Hannover, MPI for Gravitational Physics)

[75] Vacher M, Steinberg L, Jenkins A J, Bearpark M J and Robb M A 2015 Electron dynamics following photoionization: decoherence due to the nuclear-wave-packet width *Phys. Rev. A* **92** 040502(R)

[76] Hollstein M, Santra R and Pfannkuche D 2017 Correlation-driven charge migration following double ionization and attosecond transient absorption spectroscopy *Phys. Rev. A* **95** 053411

[77] Forney D, Thompson W E and Jacox M E 1992 The vibrational spectra of molecular ions isolated in solid neon. IX. HCN^+, HNC^+ and CN^- *J. Chem. Phys.* **97** 1664–74

[78] Shimanouchi T 2021 Molecular vibrational frequencies *NIST Chemistry WebBook, NIST Standard Reference Database Number* vol 69 eds P Linstrom and W G Mallard (Gaithersburg MD: National Institute of Standards and Technology) (https://doi.org/10.18434/T4D303)

[79] Fehér M, Salud C and Maier J P 1991 The infrared laser spectrum of the ν_1 band of CCN *J. Mol. Spectrosc.* **145** 246–50

[80] Mebel A M and Kaiser R I 2002 The formation of interstellar C_2N isomers in circumstellar envelopes of carbon stars: an *ab initio* study *Astrophys. J.* **564** 787–91

[81] Dhaouadi Z *et al* 1993 Vibrational motions of bases of nucleic acids as revealed by neutron inelastic scattering and resonance Raman spectroscopy. 1. Adenine and its deuterated species *J. Phys. Chem.* **97** 1074–84

[82] Laamiri K, Garcia G A, Nahon L, Ben Houria A, Feifel R and Hochlaf M 2022 Threshold photoelectron spectroscopy of 9-methyladenine: theory and experiment *Phys. Chem. Chem. Phys.* **24** 3523–31

[83] Lin C-K, Li M-C, Yamaki M, Hayashi M and Lin S H 2010 A theoretical study on the spectroscopy and the radiative and non-radiative relaxation rate constants of the $S_0^1A_1-S_1^1A_2$ vibronic transitions of formaldehyde *Phys. Chem. Chem. Phys.* **12** 11432

[84] Rodes A, Rueda M, Prieto F, Prado C, Feliu J M and Aldaz A 2009 Adenine adsorption at single crystal and thin-film gold electrodes: an *in situ* infrared spectroscopy study *J. Phys. Chem. C* **113** 18784–94

[85] Lopes R P, Valero R, Tomkinson J, Marques M P M and de Carvalho L A E B 2013 Applying vibrational spectroscopy to the study of nucleobases—adenine as a case-study *New J. Chem.* **37** 2691

[86] Nowak M J, Lapinski L, Kwiatkowski J S and Leszczyński J 1996 Molecular structure and infrared spectra of adenine. Experimental matrix isolation and density functional theory study of adenine ^{15}N isotopomers *J. Phys. Chem.* **100** 3527–34

[87] Scargle J D 1982 Studies in astronomical time series analysis. II. Statistical aspects of spectral analysis of unevenly spaced data *Astrophys. J.* **263** 835–53

[88] Burnham K P and Anderson D R 2004 Multimodel inference *Sociol. Methods Res.* **33** 261–304

[89] Runge E and Gross E K U 1984 Density-functional theory for time-dependent systems *Phys. Rev. Lett.* **52** 997–1000

[90] Marques M A L, Maitra N T, Nogueira F M S, Gross E K U and Rubio A 2012 *Fundamentals of Time-Dependent Density Functional Theory* (Berlin: Springer)

[91] Alonso J L, Andrade X, Echenique P, Falceto F, Prada-Gracia D and Rubio A 2008 Efficient formalism for large-scale *ab initio* molecular dynamics based on time-dependent density functional theory *Phys. Rev. Lett.* **101** 096403

[92] Andrade X, Castro A, Zueco D, Alonso J L, Echenique P, Falceto F and Rubio A 2009 Modified Ehrenfest formalism for efficient large-scale *ab initio* molecular dynamics *J. Chem. Theory Comput.* **5** 728–42

[93] Andrade X *et al* 2015 Real-space grids and the octopus code as tools for the development of new simulation approaches for electronic systems *Phys. Chem. Chem. Phys.* **17** 31371–96

[94] Tancogne-Dejean N *et al* 2020 Octopus, a computational framework for exploring light-driven phenomena and quantum dynamics in extended and finite systems *J. Chem. Phys.* **152** 124119

[95] Stefanucci G and Van Leeuwen R 2013 *Nonequilibrium Many-Body Theory of Quantum Systems: A Modern Introduction* (Cambridge: Cambridge University Press)